Development of Anthropomorphic Multi-D.O.F. Master-Slave Arm for Mutual Telexistence

Riichiro Tadakuma, Yoshiaki Asahara, Hiroyuki Kajimoto,
Naoki Kawakami, and Susumu Tachi, *Member*, *IEEE*

Abstract—We developed a robotic arm for a master-slave system to support "mutual telexistence," which realizes remote dexterous manipulation tasks and close physical communication with other people using gestures. In this paper, we describe the specifications of the experimental setup of the master-slave arm to demonstrate the feasibility of the mutual telexistence concept. We developed the master arm of a telexistence robot for interpersonal communication. The last degree of the 7-degree-of-freedom slave arm is resolved by placing a small orientation sensor on the operator's arm. This master arm is made light and impedance control is applied in order to grant the operator as much freedom of movement as possible. For this development stage, we compared three control methods and confirmed that the impedance control method is the most appropriate to this system.

Index Terms—Telexistence, virtual reality, force feedback, bilateral impedance control.

1 Introduction

We developed a robotic arm for a master-slave system to support "mutual telexistence," which realizes remote dexterous manipulation tasks and close physical communication with other people using gestures. In this paper, we describe the specifications of the experimental setup of the master-slave arm to demonstrate the feasibility of the mutual telexistence concept. We developed the master arm of a telexistence robot for interpersonal communication. To facilitate the operator's arm motions, the master arm was designed as a 6-degree-of-freedom structure, thus avoiding interference with the operator's arm, particularly the elbow. The last degree of the 7-degree-of-freedom slave arm is resolved by placing a small orientation sensor on the operator's arm. This master arm is made light and impedance control is applied in order to grant the operator as much freedom of movement as possible.

2 TELESAR I for Telexistence

It has long been a desire of human beings to project themselves into a remote environment, i.e., to have a sensation of presence in a remote place.

The concept of projecting ourselves by using robots is called telexistence (tele-existence) [1], [2], [3], [4]. The first telexistence master-slave system "TELESAR (Telexistence Surrogate Anthropomophic Robot) I" is shown in Fig. 1.

The second prototype of a telexistence master-slave system for remote manipulation experiments is being designed and developed with improved technology. The robot built for this system is called "TELESAR II." We focus on producing human-like, realistic movement for TELESAR II.

• *The authors are with the Department of Physics and Computing (IPC), Graduate School of Information Science and Technology (IST), University of Tokyo, 7-3-1 Hongo, Bunkyo-ku, Tokyo, 113-8656 Japan.*
E-mail: {tadakuma, asahara, kaji, kawakami, tachi}@star.t.u-tokyo.ac.jp.

Manuscript received 7 Dec. 2004; revised 25 Mar. 2005; accepted 24 May 2005; published online 8 Sept. 2005.
For information on obtaining reprints of this article, please send e-mail to: tvcg@computer.org, and reference IEEECS Log Number TVCGSI-0235-1204.

3 The Mechanism of the Master-Slave Arm of TELESAR II

3.1 Slave Arm for Mutual Telexistence

We have been progressively developing a complete anthropomorphic seven degrees of freedom (7-DOF) redundant arm for a master-slave system to support mutual telexistence. This area of field robotics places special demands on the system because it must be endowed with human-like shape and movement and is also safe for use in everyday environments with on-going human contact.

3.2 Previous Work

Many anthropomorphic 7-DOF redundant arms of humanoid robots have already been designed and built to replicate human skills. One of the first was the "Extreme Condition Working Robot" of Mitsubishi Heavy Industries Ltd. for the Japanese National Project on Advanced Robot Technology [5]. Another example was the MIA arm of Waseda University [6], designed to realize compliant motion.

Two of the full-size humanoid robot systems from Honda, called P2 and P3, have anthropomorphic 7-DOF arms [7]. H6 and ISAMU, built by the University of Tokyo and Kawada Industries, Inc., also have 7-DOF redundant arms [8], [9], [10]. However, these arms' first vertical yaw joints in their shoulders have a large offset to enlarge the motion space, so they are a bit different from normal anthropomorphic robotic arms.

Another example was built by SARCOS Research Corp. [11]. The robot's body was anchored at the waist and most of its joints were actuated by hydraulic pumps using oil pressure, so it is infeasible for use in field robotics tasks such as moving around in everyday settings.

The most recent example is NASA's Robonaut [12], [13], [14]. It is a human-scale manipulator designed to fit within the exterior volume of an astronaut's suit and to realize

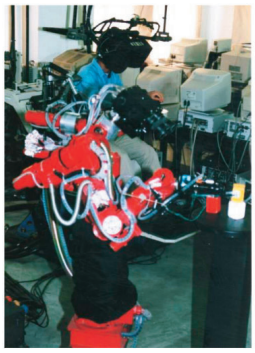

Fig. 1. The first telexistence master-slave system "TELESAT I."

thermal endurance to cope with eight hours of Extra-Vehicular Activity (EVA).

3.3 Mechanical Design of the Slave Arm

The arm we developed was designed to be as light as possible in order to move quickly and to be safe for human use. By uniting the housing parts of the harmonic drive gear system with other parts, such as the rotational axes of joints, we made the whole mechanism of the arm very light. Moreover, by this design, we succeeded in making the arm mechanism as slim as the outer human arm. The distribution of the joints of the arm replicates the human arm's structure in order to make it easy to operate by telexistence using kinesthetic sensation. This structure is also useful for interaction with people without a sense of incongruity. A complete view of the arm is shown in Fig. 2.

In order to confirm the validity of our slave arm's functions, we compared it with other anthropomorphic 7-DOF arms. For comparison, we chose designs whose specification details were released in references and the three axes of joints in their shoulders and wrists cross at one point, just like the structure of the human arm and our slave arm. The result is shown in Table 1 (human data was taken from [15], [16], [17]). The degree values of this table are displayed considering the posture of the left picture of Fig. 2 as a neutral point.

Through this comparison, we confirmed that our new slave arm supports sufficient payload and speed for mutual telexistence using gestures and, since it is much lighter than existing arms, the potential danger of injury due to malfunction is also greatly reduced. At the same time, our slave arm has a larger mobility range in the joints above the elbow.

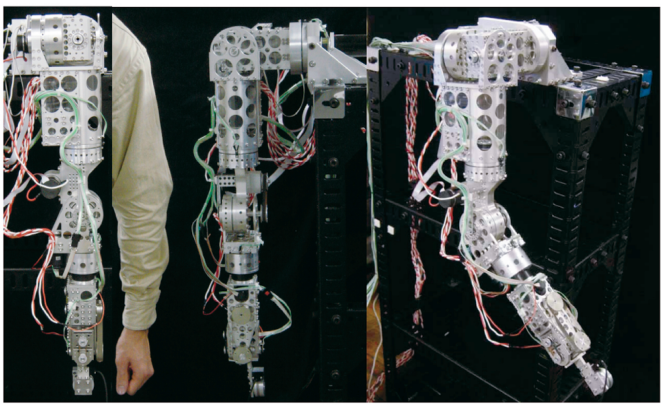

Fig. 2. The whole view of the slave arm of TELESAR II.

TABLE 1
Comparing Designs of the New Slave Arm

Robot			New slave arm (Human arm)	Mitsubishi Extreme Condition Robot	Waseda MIA arm
Weight [kg]			7.3	34.2	25
Mobility range [deg]	Shoulder	J1	-180/+180 (-60/+180)	-90/+180	-50/+180
		J2	0/+180 (0/+165)	-5/+165	-35/+90
		J3	-180/+180 (0/+100)	-100/+100	-90/+90
	Elbow	J4	0/+135 (0/+130)	0/+135	0/+125
	Wrist	J5	-180/+180 (0/+180)	-70/+220	-90/+90
		J6	-35/+35 (-35/+35)	-45/+85	-90/+75
		J7	-35/+35 (-35/+35)	-65/+65	-32/+32
Payload [kg]			0.5	5	0.5
Velocity [m/s]			1.2	2.8	1

The reduction ratio of the harmonic drive of each joint of the slave arm was set to 50 to maintain back-drivability. The actuators for the arm are shown in Table 2.

The maximum force at the tip of the slave arm is 164 [N].

The maximum torque of each joint of the slave arm is shown in Table 3.

3.4 Control System of the Slave Arm

Fig. 3 shows the control system for the slave arm. The motor driver controls the DC motors in the joints with a torque control mode according to commands from the DA board. The angular velocity and the posture of each joint are measured with an encoder attached to the motor. The neutral point of each joint is defined by potentiometers or photo-interrupters, whose signals are read by the AD board. The slave arm's control system is connected to the master arm system through shared memory. The control system for the master arm is the same as the slave arm system.

3.5 Master Arm for Mutual Telexistence

In order to realize a telexistence robot that produces a convincing sense of presence, it is indispensable to capture motion from an operator without restraining his or her free movement and to correctly display useful force information to the operator at the same time.

TABLE 2
Actuators of the Slave Arm

Shoulder Motor	J1, J2	150 [W]
	J3	90 [W]
Elbow Motor	J4	90 [W]
Wrist Motor	J5, J6, J7	17.5 [W]
Reduction Ratio		50

TABLE 3
The Maximum Torque of Each Joint of the Slave Arm

Number of the joint	Maximum torque of the joint [Nm]
JT1	91.6
JT2	91.6
JT3	38.0
JT4	38.0
JT5	5.56
JT6	5.56
JT7	5.56

To satisfy these criteria, we developed a master arm with 6 DOF that has an exoskeleton-type structure and assessed its performance and efficacy through experiment. We describe here the mechanism design and feasibility evaluation.

3.6 Mechanical Design of the Master Arm

A general anthropomorphic slave arm is built as a 7-DOF mechanism that has the same structure as that of a person. The master arm used as the operation system is also usually given a 7-DOF structure, but it is difficult to realize free motion of the operator because it tends to restrain the operator's elbow mechanically.

From the viewpoint of simplification of function and control, we considered its high rigidity and the fact that the force to be applied to the operator's hand is along at most six axes and we designed the master arm to specialize in the force presentation function in these six axes and also made its mechanism 6-DOF.

Because the master arm has the cantilever beam structure as serial links, if the degree of freedom of the master arm increases, the length of the cantilever beam and the total weight of the actuators also increase, driving down the rigidity and stability of the master arm.

Since the measurable movement of the master arm that follows the operator's hand has 6 DOF, we decided to use a new lightweight posture sensor composed of an acceleration sensor to measure the final DOF, which is critical to identifying the posture of the operator's whole arm.

Altogether, the master arm serves as a master system of 7 DOF for measurement of the arm's posture and 6 DOF for force presentation. Since the posture sensor is very light compared with mechanical restraints on the operator's elbow, the sensor enables much freer movement of his or her arm without any undesirable load on it.

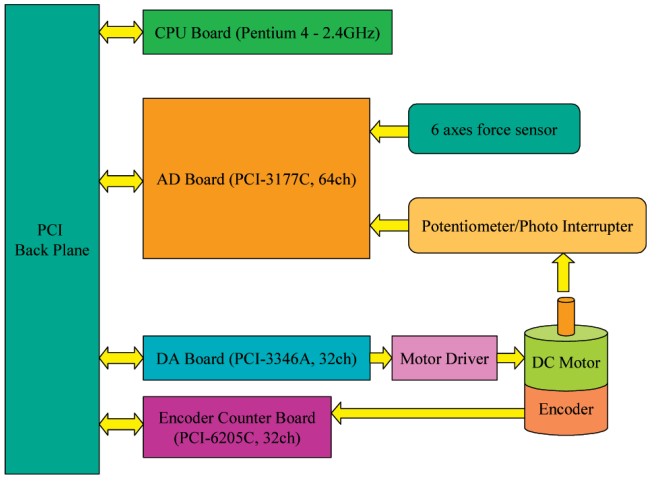

Fig. 3. Control system for the slave arm.

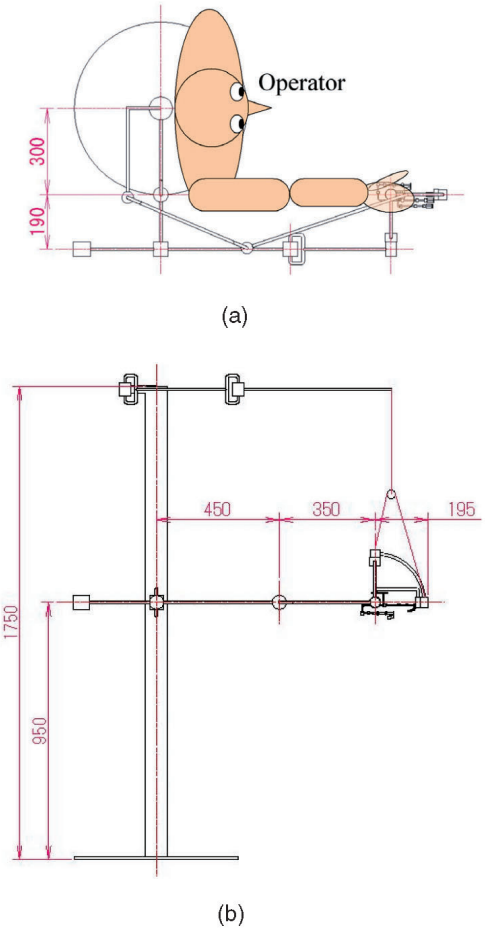

Fig. 4. The whole schematic of the master arm. (a) Plane figure of the master arm. (b) Front view of the master arm.

We decided to use the exoskeleton structure because we considered that it could be widely adapted for the movement of an operator with minimal size requirements, which is an essential characteristic to correspond to a human's various actions in everyday life.

The whole schematic of the master arm is shown in Fig. 4. The operator's backbone is located near the center of the circle in Fig. 4. The 190 mm offset between the shoulder joint of the master arm and the elbow joint is the clearance for avoiding interference of the master arm and the operator's elbow and the turning radius of the gimbal mechanism at the tip of the arm in Fig. 4 is the same length as the offset.

The whole view of the developed master arm described in this paper is shown in Fig. 5.

A potentiometer and an encoder are installed in each joint and the operator's initial posture is computed from the output signals from the potentiometers and, during movement, his or her arm's joint angles and angular velocities are computed from the output signals from the encoders.

The three axes of the joints in the master arm's wrist cross at one point, as shown in Fig. 6, and a 6-axes force sensor (MINI 4/20, made in BL AUTOTEC) is attached to that point. Output signals from this sensor are used to measure the force that works between the wrist of the master arm and the operator in the direction of the rotating

Fig. 5. The master arm of TELESAR II.

axis and the torque that works around the axis. The tip of the master arm is currently just a simple grip, but, in the near future, we will attach the exoskeleton-type multi-fingered master hand to the tip and develop a bilateral system including fingers.

Specifications of the master arm are shown in Table 4. The degree values of this table are displayed considering the posture of Fig. 4 as a neutral point.

The gear system of each joint of the master arm is composed of a combination of precise spur gears of module 0.3, comparatively small size of the teeth, as shown in Fig. 7.

In the assembly process, the tooth outlines of the coupled gears were precisely fitted to ensure high back-drivability and even high reduction ratio of each joint, so the arm can be used as a passive master arm.

We made the dynamic model of frictional resistance in the gear system of all joints with identification experiments and use that model for precise impedance control.

A gravity compensation system is realized by hanging the tip of the master arm with wire, which enables the manipulator to exhibit maximum performance. The tension of the wire is 20.6 [N]. Because of this gravity compensation system, the actuators of the master arm's joints don't have to compensate for the gravitational torque applied to the master arm. Therefore, the master arm is able to present forces to the operator's hand with small output torque and high accuracy. The mechanism that suspends the arm tip component with a wire is constituted as shown below. A passive link that has two joints is attached above the master arm, as shown in Fig. 5. The constant force spring passes inside the link, as shown in Fig. 8. Constant tension works on the wire by passing it through the pulley at the tip of the spring. The wire is attached to the tip of the master arm. Since the joints of this link are parallel to the direction of gravity, the link can follow the master arm smoothly with the wire that circulates through it, while maintaining a horizontal posture.

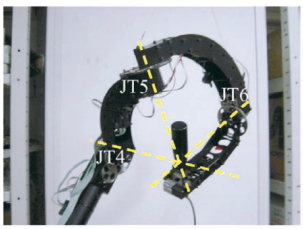

Fig. 6. The three axes of the wrist cross at one point.

TABLE 4
Specifications of the Master Arm

	Mobility range of each joint	Output of the motor	Reduction ratio of the gear system
JT1	-75/+60 [deg]	150 [W]	125
JT2	-30/+100 [deg]	150 [W]	625/6
JT3	-140/+0 [deg]	36 [W]	625/6
JT4	-180/+180 [deg]	18 [W]	525/4
JT5	-50/+230 [deg]	18 [W]	525/4
JT6	-180/+180 [deg]	18 [W]	525/4

The maximum force at the tip of the master arm is 239 [N]. The maximum torque of each joint of the master arm is shown in Table 5.

4 Control Methods of the Master-Slave Arm of TELESAR II

4.1 Concept of Bilateral Impedance Control as Dual Motion Transmission Method

We adapted bilateral impedance control for TELESAR II. The basic principle of the impedance control type master-slave system is to give seemingly equivalent impedance to both master and slave. Furthermore, by minimizing its impedance, the master arm places only a slight load onto the operator's arm and he or she can perform a wide variety of gestures and other body movement expressions without being hindered.

Here, we explain the presently adopted Dual Motion Transmission Method of the bilateral impedance control that exchanges movement information between the master and the slave [18]. In this control method, the master's force is equal to the slave's and exact force presentation can be performed in contact work. The conceptual image of Dual Motion Transmission Method of the bilateral impedance control is shown in Fig. 9. In this control method, both the master arm and slave arm have force sensors at their wrists.

Specifically, control is performed based on the movement equations below:

For the master:

$$F_o = M_d\ddot{X}_m + B_d\dot{X}_m + K_dX_m - F_{tm}. \quad (1)$$

For the slave:

$$F_{ts} + M_d\ddot{X}_s + B_d\dot{X}_s + K_dX_s + F_e. \quad (2)$$

Here, (M_d, B_d, K_d) mean the target impedance parameters of the master arm and the slave arm, F_o means the

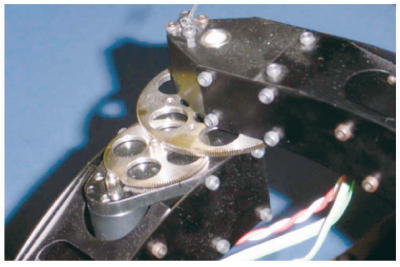

Fig. 7. The gear system of the joint of the master arm.

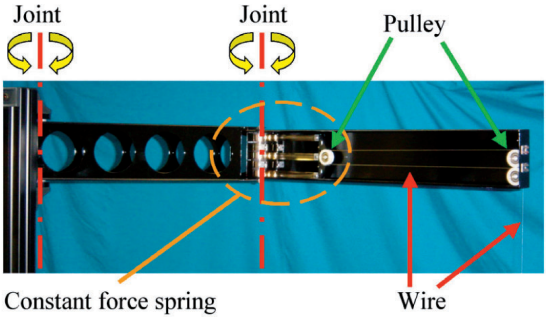

Fig. 8. The mechanism of the passive link for gravity compensation.

operational force to the operator, F_{tm} and F_{ts} mean the inner torque of the master and the slave, F_e means the power that works from the object to the slave arm, X_m and X_s mean the posture vectors of the master and the slave.

In the Dual Motion Transmission Method, the control methods are as shown below.

For the master:

$$F_{tm} = M_d\ddot{X}_s + B_d\dot{X}_s + K_dX_s. \tag{3}$$

For the slave:

$$F_{ts} = M_d\ddot{X}_m + B_d\dot{X}_m + K_dX_m. \tag{4}$$

From (1)-(4), the relationship between F_o and F_e is derived as shown below:

$$F_o = F_e = M_d(\ddot{X}_m - \ddot{X}_s) + B_d(\dot{X}_m - \dot{X}_s) + K_d(X_m - X_s). \tag{5}$$

The block diagram of the adopted impedance control system is shown in Fig. 10. The sequence of this block diagram is as follows:

1. With the encoder attached to each joint of the arm, the joint angle Θ and joint angular velocity $\dot{\Theta}$ are measured and, with the 6-axes force sensor attached to the wrist, the external force FEXT applied to the wrist is measured.
2. From the measured joint angle Θ, the position and orientation of the wrist X in Cartesian space is calculated with forward kinematics $L(\Theta)$ and $\dot{X}$ is also calculated from the equation of $\dot{X} = J\dot{\Theta}$ with Jacobian matrix J.
3. Equation (6) shows the relationship of impedance. From this equation, the acceleration $\ddot{X}$ is calculated as shown in (7).

TABLE 5
The Maximum Torque of Each Joint of the Master Arm

Number of the joint	Maximum torque of the joint [Nm]
JT1	229
JT2	191
JT3	44.9
JT4	8.97
JT5	8.97
JT6	8.97

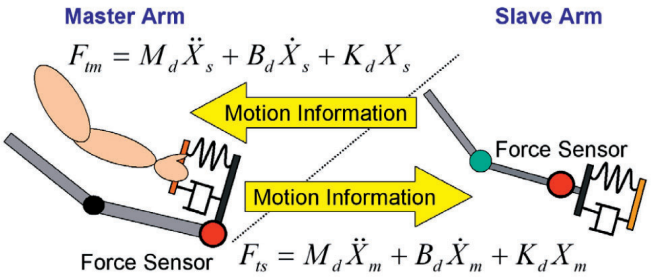

Fig. 9. The conceptual image of the Dual Motion Transmission Method of the bilateral impedance control.

$$F_{EXT} = M_d\ddot{X} + B_d(\dot{X} - \dot{X}_d) + K_d(X - X_d), \tag{6}$$

$$\ddot{X} = M_d^{-1}F_{EXT} - M_d^{-1}B_d(\dot{X} - \dot{X}_d) - M_d^{-1}K_d(X - X_d). \tag{7}$$

4. Equation (8) shows the relationship between Cartesian space and the joint space.

$$\dot{X} = J\dot{\Theta}. \tag{8}$$

5. The time differentiation of (8) gives the angular acceleration $\ddot{\Theta}$, as shown below.

$$\ddot{X} = J\ddot{\Theta} + \dot{J}\dot{\Theta}, \tag{9}$$

$$\ddot{\Theta} = J^{-1}\ddot{X} - J^{-1}\dot{J}\dot{\Theta}. \tag{10}$$

6. Resolve inverse dynamics by the Newton-Euler method with the parameters of the arm's motion and force, $(\ddot{\Theta}, \dot{\Theta}, \Theta, F_{EXT})$, and the output of this calculation, torque τ, is to be used as the torque for each actuator of the arm.

The actual dynamics of the arm, $\left(M(\Theta), V(\Theta, \dot{\Theta}), G(\Theta)\right)$ in the third block is calculated from the parameters of inertia of the arm. These parameters were calculated by the three-dimensional CAD system used to design the master and slave arms. In the case of the master arm, X is X_m and, in the case of the slave arm, X is X_s. For both the master and slave arms, $(X_d, \dot{X}_d)$ denotes information coming from the opposing arm.

4.2 Modified Bilateral Impedance Control for 7 DOF Anthropomorphic Slave Arm

In the bilateral impedance control between the 6 DOF master arm and our new anthropomorphic 7 DOF slave arm, the Jacobian matrix is rank deficient (6×7) and the inverse Jacobian matrix in the second block of the impedance control diagram of Fig. 10 cannot be calculated. So, we opted to use the posture sensor that can measure the position and orientation of the operator's elbow. This posture sensor is composed of an acceleration sensor that measures its own posture with the direction of the gravitational acceleration. We attached the sensor to the operator's upper arm and, with the information from this sensor, we measure the angle of one joint of the operator's shoulder and control the same joint of the anthropomorphic

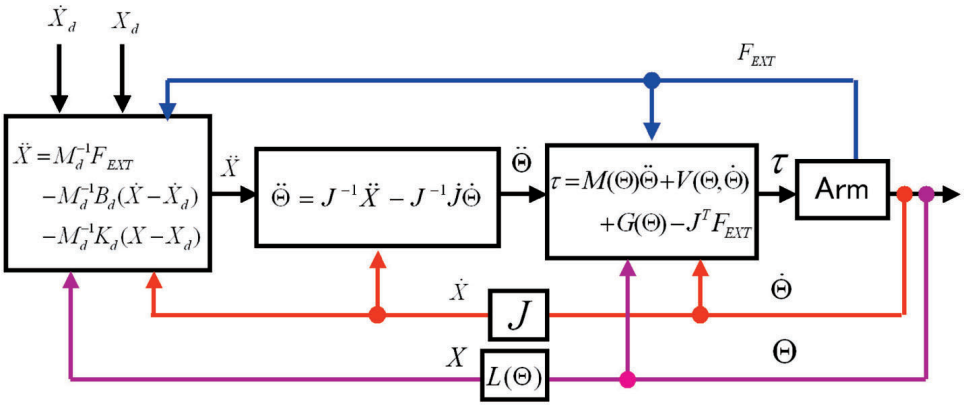

Fig. 10. The block diagram of the adopted impedance control.

7 DOF slave arm in PD control and control the other six joints in impedance control. In this case, the Jacobian matrix has full rank (6×6) and its inverse in the second block of the diagram may now be calculated. The concept of this modified bilateral impedance control is shown in Fig. 11.

In this way, we can control the anthropomorphic 7 DOF slave arm with a redundant degree of freedom in bilateral impedance control.

In this measurement method, the master side has 7 DOF for position and orientation, while it has 6 DOF for force feedback, as shown in Fig. 11. As the operator's arm can be regarded as a redundant 7 DOF manipulator, conventional methods to solve inverse kinematics of the redundant arm can be applied to measure the operator's posture. One popular method is to define a swivel angle of an arc of a circle, which the elbow traces, lying on a plane whose normal is parallel to the wrist-to-shoulder axis. Given the wrist position, orientation, and elbow swivel angle, the algorithm can compute the joint angles analytically. Note that the wrist position and orientation of the operator is identical to that of the master manipulator. In order to get the remaining information (swivel angle), we used the acceleration sensor (ADXL202E, Analog Devices, Inc.) attached to the operator's upper arm. The sensor has a high enough frequency response (1kHz), while its small size and light weight allow the operator to move freely. We used an axis of the sensor corresponding to the change of the swivel angle, as shown in Fig. 12. The method to solve inverse kinematics of the slave arm is as follows: The origin $(0, 0, 0)$ is coincident with the shoulder position and (L_1, L_2, L_3) denotes the length of the upper arm, lower arm, and the distance from the goal position to the shoulder of the slave arm. First, the goal position $\mathbf{P}$ and orientation $\mathbf{R}$ (rotation matrix) of the slave arm's wrist are determined by forward kinematics of master arm. The joint angle of the elbow θ_4 is then determined geometrically, as shown in Fig. 13.

In Fig. 13, $\mathbf{n}$ is a unit vector from the shoulder to the wrist. $\mathbf{u}$ and $\mathbf{v}$ are unit vectors forming a local coordinate system for the plane containing the circle traced by the elbow. $\mathbf{u}$ is determined arbitrarily to correspond to $\phi = 0$. Then, $\mathbf{v}$ is set as $\mathbf{v} = \mathbf{n} \times \mathbf{u}$. Similarly to θ_4, α is determined and the center of the circle $\mathbf{c}$ traced by the elbow and its radius r can be computed as

$$\cos\alpha = \frac{L_1^2 + L_3^2 - L_2^2}{2L_1L_3}, \tag{11}$$

$$\mathbf{c} = L_1 \cos\alpha \mathbf{n}, r = L_1 \sin\alpha. \tag{12}$$

If we set $\mathbf{u}$ as the direction such that the output of the acceleration sensor a is equal to the gravitational acceleration g,

$$\mathbf{u} = \frac{(n_z \quad 0 \quad -n_x)^T}{\sqrt{n_x^2 + n_z^2}}, \tag{13}$$

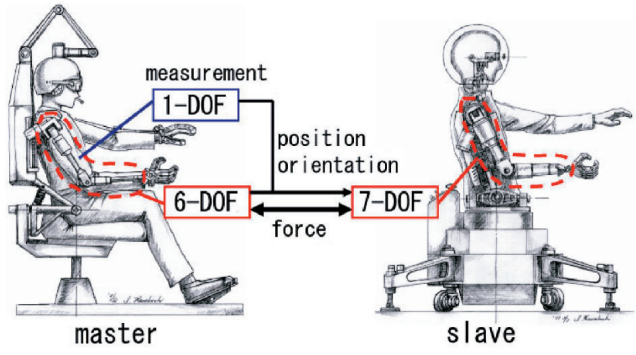

Fig. 11. Concept of modified bilateral impedance control for the master-slave system with different degrees of freedom.

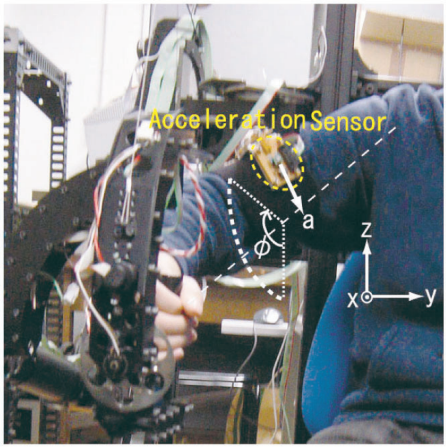

Fig. 12. Swivel angle, an acceleration sensor attached to an operator's upper arm, and its axis a.

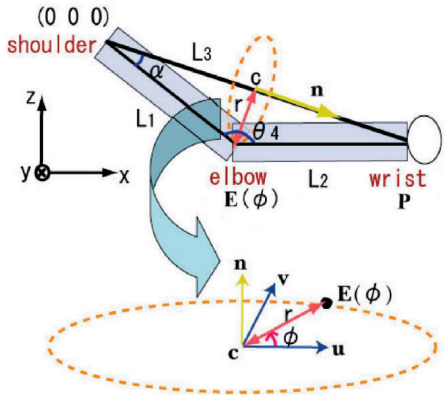

Fig. 13. Geometric relationship between shoulder, elbow, and wrist.

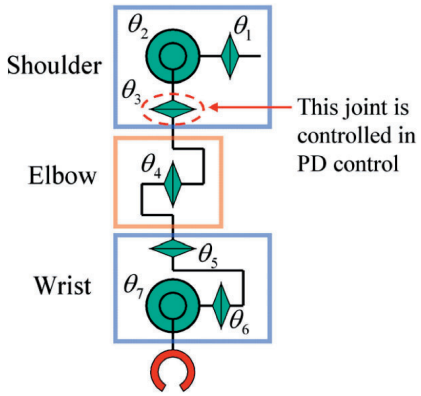

Fig. 14. Configuration of the human arm and the slave arm.

the swivel angle ϕ is obtained as

$$\sin\phi = \frac{a}{g}. \tag{14}$$

Then, the elbow position $\mathbf{E}(\phi)$ is given by

$$\mathbf{E}(\phi) = \mathbf{c} + r(\cos\phi\mathbf{u} + \sin\phi\mathbf{v}). \tag{15}$$

From the relation between this elbow position $\mathbf{E}(\phi)$ and wrist position $\mathbf{P}$, three joints angles of the shoulder, $\theta_1 \sim \theta_3$, are determined. Next, from the orientation $\mathbf{R}$ of the wrist, three joint angles of the wrist, $\theta_5 \sim \theta_7$, are determined.

As described above, we can solve inverse kinematics of the redundant slave arm that satisfies the wrist's position and orientation obtained by the master arm and elbow position computed from an acceleration sensor's output. With this method, the slave arm can replicate the operator's motion and posture even though the master arm has a different kinematic configuration from the slave arm and the operator's arm.

With this method of inverse kinematics using the elbow posture sensor, we can get all the joint angles of the operator's arm ($\theta_1 \sim \theta_7$ in Fig. 14). Among these joint angles, we decided to use θ_3, meaning the operator's arm's roll joint angle at the shoulder to control the slave arm's roll joint at its shoulder with PD control, and to control the other six joints of the slave arm with impedance control. We use the Newton-Euler method of inverse dynamics to calculate the torque for each joint of the slave arm in the third block of the block diagram of the impedance control (Fig. 10) by setting the angular acceleration $\ddot{\theta}_k$ to zero in order to control the one joint with PD control. So, we choose the joint whose angular acceleration, on average, is the smallest of all joints of the human wrist and shoulder that are related to the redundant degree of freedom's posture to make the interference of PD control with impedance control as small as possible. To find this type of joint, we analyzed the angular accelerations of all joints of a human arm in several gestures with an optical motion capture system, OPTO-TRAK. After some experimentation and comparison, we found the angular acceleration of the roll joint of human shoulder is the smallest on average. So, we decided to control this joint of the slave arm with PD control. In this control method, the Jacobian matrix becomes a full rank matrix (6×6) and we can calculate its inverse matrix for the second block of the block diagram of impedance control.

In this way, the equation that shows the relationship between Cartesian space and the joint space changes from

$$\left(\dot{x}, \dot{y}, \dot{z}, \dot{\alpha}, \dot{\beta}, \dot{\gamma}\right)^T = \mathbf{J}\left(\dot{\theta}_1, \dot{\theta}_2, \dot{\theta}_3, \dot{\theta}_4, \dot{\theta}_5, \dot{\theta}_6, \dot{\theta}_7\right)^T \tag{16}$$

to

$$\left(\dot{x}, \dot{y}, \dot{z}, \dot{\alpha}, \dot{\beta}, \dot{\gamma}\right)^T = \mathbf{J}\left(\dot{\theta}_1, \dot{\theta}_2, \quad \dot{\theta}_4, \dot{\theta}_5, \dot{\theta}_6, \dot{\theta}_7\right)^T \tag{17}$$

in impedance control. In this case, $\ddot{\theta}_3 = 0$. $\left(\dot{x}, \dot{y}, \dot{z}, \dot{\alpha}, \dot{\beta}, \dot{\gamma}\right)$ mean the time differentiations of the position and orientation of the operator's hand. This control method is used in bilateral impedance control between the 6 DOF master arm and the anthropomorphic 7 DOF slave arm in the last part of Section 4.

Another merit of bilateral impedance concerns operation safety. For contact operations of the slave arm with another person, the operator can feel the force from the person with a high sense of reality, so the potential danger of giving him or her superfluous force can be avoided.

If we control the master-slave system with a Dual Motion Transmission Method, in a state where the slave arm is moved without applying external force from an object in the outer environment, since the master's force and the slave's are not equal, the operator receives the force by the product of target impedance and the posture error. However, making target impedance as small as possible can minimize undesirable load, unlike other control methods.

4.3 Verification of Bilateral Impedance Control

In order to verify the optimality of this system, we conducted simple comparison experiments with symmetry and force feedback, which are general control method types.

The symmetry type is a control method in which the master and the slave transmit their posture information to each other and apply a suitable gain according to the difference of their postures to produce a torque output, as shown in Fig. 15.

Specifically, control is performed based on the movement equation and the control equations shown below:

For the master:

$$F_0 = M_m\ddot{X}_m + B_m\dot{X}_m + F_{tm}, \tag{18}$$

$$F_{tm} = K_p(X_m - X_s) + K_v\left(\dot{X}_m - \dot{X}_s\right). \tag{19}$$

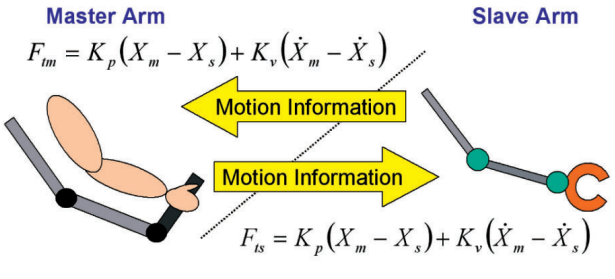

Fig. 15. The conceptual image of Symmetry type control.

For the slave:

$$F_{ts} = M_s\ddot{X}_s + B_s\dot{X}_s + F_e, \tag{20}$$

$$F_{ts} = K_p(X_m - X_s) + K_v(\dot{X}_m - \dot{X}_s). \tag{21}$$

Here, (M_m, B_m) mean the master arm's impedance parameters and (M_s, B_s) mean the slave arm's impedance parameters. K_v and K_p are the feedback gains of the velocity and the position.

The force presented to the operator is as shown below:

$$F_0 = M_m\ddot{X}_m + B_m\dot{X}_m + M_s\ddot{X}_s + B_s\dot{X}_s + F_e. \tag{22}$$

The operator has to cope with the inertial and velocity-related forces from both the master arm and the slave arm in the symmetry type.

The force feedback type is a control method in which the master transmits posture information to the slave and the slave transmits force information to the master, as shown in Fig. 16. In this control method, both the master arm and slave arm have force sensors at their wrists. The master receives the torque command value from the product of the suitable gain and the difference of the master's force and the slave's and the slave receives the torque command value from the product of the gain and the difference between the master's posture and the slave's.

Specifically, control is performed based on the movement equation and the control equation shown below:

For the master:

$$F_0 = M_m\ddot{X}_m + B_m\dot{X}_m + F_{tm}, \tag{23}$$

$$F_{tm} = K_f(F_e - F_0). \tag{24}$$

For the slave:

$$F_{ts} = M_s\ddot{X}_s + B_s\dot{X}_s + F_e, \tag{25}$$

$$F_{ts} = K_p(X_m - X_s) + K_v(\dot{X}_m - \dot{X}_s). \tag{26}$$

Here, K_f is the feedback gain of the force. The force presented to the operator is as shown below:

$$F_0 = \frac{1}{1+K_f}(M_m\ddot{X}_m + B_m\dot{X}_m) + \frac{K_f}{1+K_f}F_e. \tag{27}$$

At first, we used the left arm of the master system as the virtual slave arm and used the right arm of the master system as the master arm to eliminate the mechanical difference between the master and the slave and to compare the control methods themselves.

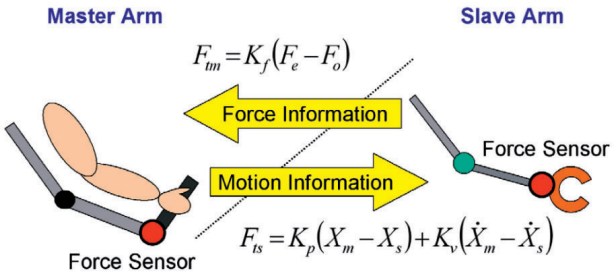

Fig. 16. The conceptual image of Force-feedback type control.

In the following text, the word "master" refers to the right arm of the master manipulator system and the word "slave" refers to its left arm.

For the first fundamental experiment, only the yaw-axes of the shoulders of the right and left master arms were moved. Master-slave control was performed such that, when the right arm is moved to the left, the left arm also moves to the left, in the same direction.

We investigated the following two concerns in this comparison experiment:

1. When the right arm (virtual master arm) is moved, how well does the slave arm follow?
2. What is the presented force when force is applied by the operator?

In all of the comparison experiments, the impedance of the arm with the impedance control type was set as $M = 6$ [kg], $B = 2$ [kgf/(m/s)], and $K = 2$ [kgf/m].

First, we describe the experiment that considered the force that works on the operator. The forces from the master arm that work on the operator in the symmetry type, the force feedback type, and the impedance control type are shown in the following three graphs (Figs. 17, 18, and 19).

In the symmetry type, if the operator provides acceleration, a large operational force is needed because of the inertia of both the master arm and the slave arm.

In the force feedback type, because the master is controlled by the force difference between the master and the slave, as shown in (24), the force that works on the operator is comparatively close to the value of the slave that does not receive any force. The reason is the slave does not receive any force from the outer environment, $F_e = 0$ and $F_{tm} = -K_f F_o$. This torque output F_{tm} reduces F_o and also decreases the difference between $F_e(= 0)$ and F_o.

In the impedance control type, the operational force is relatively small because of the reduction in inertia.

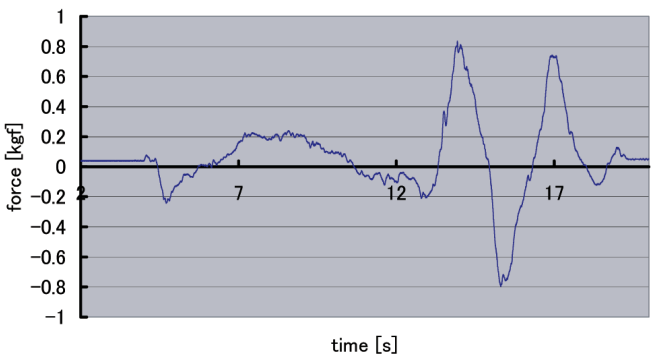

Fig. 17. Force on the operator in symmetry type.

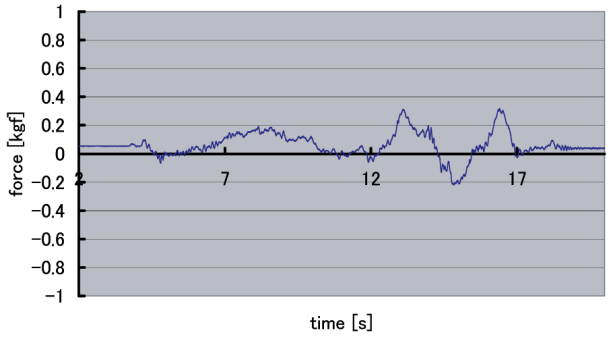

Fig. 18. Force on the operator in the force feedback type.

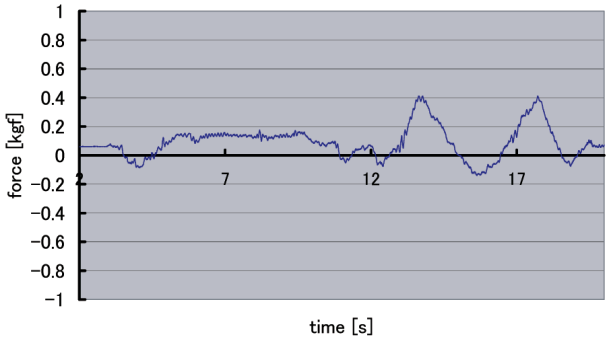

Fig. 19. Force on the operator in the impedance control type.

Almost the same force is needed in the force feedback type and the impedance control type. This is considered to be because of the identical structures of the master and the slave in this experimental system.

In addition, we conducted several experiments using only the yaw-axes of the shoulders of the right and left master arms, and classified the three control methods as shown in Table 6.

However, these results can be predicted with the control equations of the three types of control methods described in Section 4, so these experiments simply confirm each control theory. So, we conducted the second experiment using all six joints of each arm to verify the optimality of this system with bilateral impedance control. In this case, the result of the experiment is not easily predictable.

In the second experiment, we activated all six axes of the master arm and the virtual slave arm. The slave arm traced the wall and we measured the operational force and the opposing force from the wall applied to the slave arm. Results of this experiment are shown in Fig. 20.

For the symmetry type, the operational force is large because the operation itself requires large force. In the force feedback type, the virtual slave arm pushes the wall with superfluous force and the operator can't feel it. In the impedance control type, tracing with stable force was realized. So, almost the same tendency of three control methods shown in Table 6 as the results of the experiments with one joint is also shown in this experiment with six joints.

TABLE 6
Classification of Three Control Methods

	Symmetry Type	Force feedback type	Impedance control type
Following ability	Moderate	Moderate	Good
Operational force	Bad	Good	Good
Force presentation	Good	Bad	Good

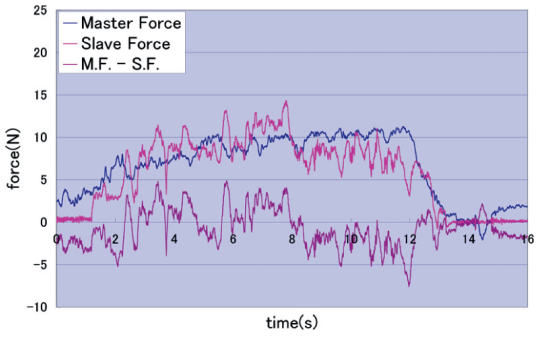

(a)

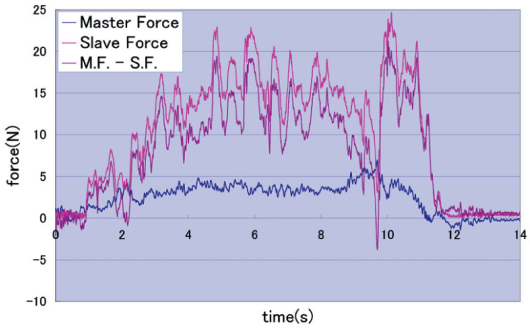

(b)

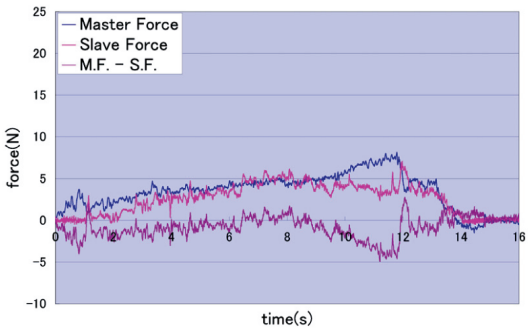

(c)

Fig. 20. Results of the second experiment of comparison. (a) Symmetry type. (b) Force feedback type. (c) Impedance control type.

In the third experiment, we checked the influence of different inertia in comparison with the symmetry and impedance control types. We attached a weight of 0.5kg to the forearm of the virtual slave arm to increase its inertia and measured the operational force. The results of this experiment are shown in Fig. 21. Compared with the increase of the operational force in the symmetry type (from 7.4 N to 9.3 N), the increase of operational force in the impedance control type is very small (from 3.7 N to 3.9 N). The inertia of the weight on the forearm of the slave arm is included in the dynamic model of the slave arm in the impedance control type and that is the reason why the operational force does not increase so much in impedance control.

As shown in the experiments described above, the characteristics of the impedance control are superior to the other two control methods. So, we decided to adapt impedance control for the master-slave system with the actual anthropomorphic slave arm.

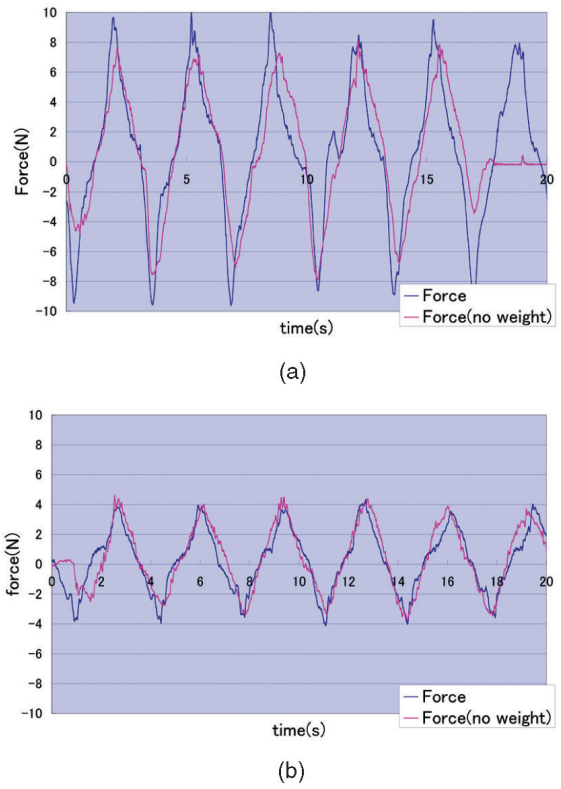

Fig. 21. Results of the third experiment of comparison. (a) Symmetry type. (b) Impedance control type.

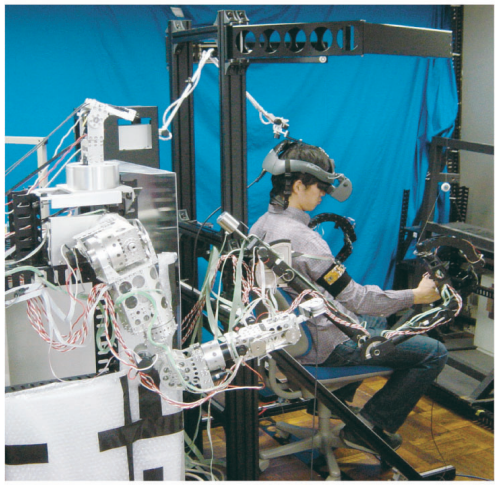

Fig. 22. The overall view of the experimental setup.

In the fourth experiment, we used the actual slave arm of TELESAR II to confirm the validity of bilateral impedance control for a master-slave arm with a different mechanical structure, such as degrees of freedom and inertia.

The overall view of the experimental setup is shown in Fig. 22. In the fourth experiment, the slave arm moved in free space and we checked the accuracy of its following ability in three axes of the universal coordinate. The results of this experiment are shown in Table 7. This table shows the maximum overshoot in the direction of each axis of the universal coordinate. As shown in this table, sufficient accuracy for gestures and communication was confirmed in this experiment.

In the fifth experiment, we checked the accuracy of force presentation of this system. The slave arm traced the wall, and we measured the operational force and the opposing force from the wall applied to the slave arm. The result of this experiment is shown in Fig. 23. Small operational force is realized, forces on the master arm and the slave arm are comparatively close and a stable trace is also realized. Namely, impedance control type is also effective in this system.

TABLE 7
Maximum Overshoot of the Slave Arm's Wrist in Universal Coordinate

X axis [mm]	11.6
Y axis [mm]	21.9
Z axis [mm]	26.8

Through all the experiments described above, the features that must be realized in a good master-slave system for telexistence were actually realized using the impedance control type, so the validity of the impedance control type was confirmed. The features were as follows:

- reproduction of the operator's work,
- precise force feedback,
- stable contact,
- gestures are enabled,
- smooth operation,
- sufficient accuracy of following ability,
- safe for humans,
- precise force feedback, and
- stable contact operation (for shaking hands, etc.).

In the final experiment, we used the master-slave head system for vision feedback. The robot head is composed of two CCD cameras and two DC motors. It has a screw mechanism to adjust the distance between the two cameras to match the distance between the two eyes of the operator. Fig. 24 shows the system diagram of the robot head.

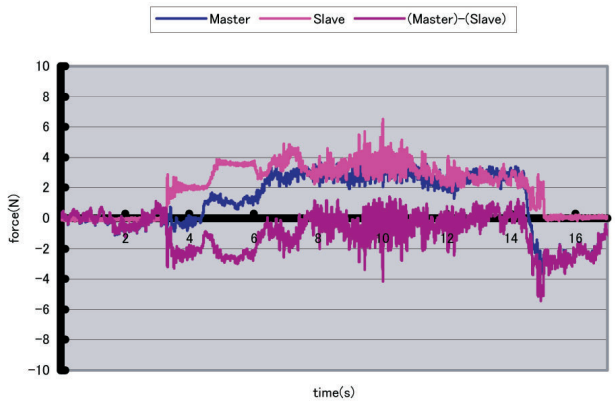

Fig. 23. The results of the experiment using the slave arm.

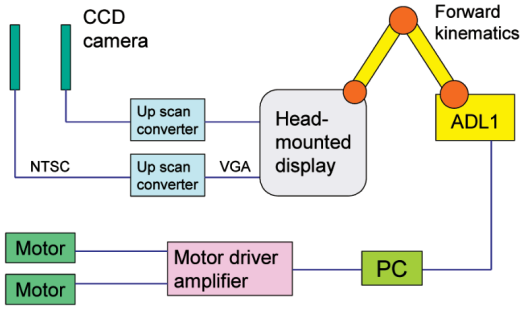

Fig. 24. The system diagram of the robot head.

CCD cameras are connected to up scan converters and vision information in NTSC format is converted to VGA format for the head-mounted display (HMD). The HMD is connected to an ADL1 that measures the orientation of the operator's head with forward kinematics.

5 Conclusion

This paper described the mechanical design and control methods of a new anthropomorphic multi-DOF master-slave arm for mutual telexistence. The validity of the bilateral impedance control was confirmed in experiments using the master arm and the slave arm. With this system, the operator will be able to move the slave robot in a remote location very smoothly with a high sense of presence.

Acknowledgments

This work has been partially supported by the project of the Japan Science and Technology Agency (JST), Core Research for Evolutional Science and Technology (CREST).

References

[1] S. Tachi, H. Arai, and T. Maeda, "Development of an Anthropomorphic Tele-Existence Slave Robot," *Proc. Int'l Conf. Advanced Mechatronics (ICAM),* pp. 385-390, 1989.

[2] S. Tachi, H. Arai, and T. Maeda, "Tele-Existence Master Slave System for Remote Manipulation," *Proc. Int'l Workshop Intelligent Robots and Systems (IROS '90),* pp. 343-348, 1990.

[3] S. Tachi, H. Arai, T. Maeda, E. Oyama, N. Tsunemoto, and Y. Inoue, "Tele-Existence Experimental System for Remote Operation with a Sensation of Presence," *Proc. Int'l Symp. Advanced Robot Technology (SART '91),* pp. 451-458, Mar. 1991.

[4] S. Tachi and K. Yasuda, "Evaluation Experiments of a Teleexistence Manipulation System," *Presence,* vol. 3, no. 1, pp. 35-44, 1994.

[5] T. Oomichi, M. Higuchi, and K. Oonishi, "Design Method of the Dexterous Fingered Manipulator," *J. Robotics Soc. Japan,* vol. 16, no. 4, pp. 508-517, 1998.

[6] T. Morita, N. Tomita, T. Ueda, and S. Sugano, "Development of Force-Controlled Robot Arm Using Mechanical Impedance Adjuster," *J. Robotics Soc. Japan,* vol. 16, no. 7, pp. 1001-1006, 1998.

[7] M. Hirose, T. Takenaka, H. Gomi, and N. Ozawa, "HUMANOID ROBOT," *J. Robotics Soc. Japan,* vol. 15, no. 7, pp. 983-985, 1997.

[8] K. Nishiwaki, T. Sugihara, S. Kagami, F. Kanehiro, M. Inaba, and H. Inoue, "Design and Development of Research Platform for Perception-Action Integration in Humanoid Robot: H6," *Proc. IEEE/RSJ Int'l Conf. Intelligent Robots and Systems,* pp. 1559-1564, 2000.

[9] S. Kagami, K. Nishiwaki, T. Sugihara, J.J. Kuffner, M. Inaba, and H. Inoue, "Design and Implementation of Software Research Platform for Humanoid Robotics: H6," *Proc. Int'l Conf. Robotics and Automation (ICRA '01),* pp. 2431-2436, 2001.

[10] S. Kagami, K. Nishiwaki, J.J. Kuffner, K. Okada, M. Inaba, and H. Inoue, "Low-Level Autonomy of Remote Operated Humanoid Robot H6 & H7," *Proc. 10th Int'l Symp. Robotics Research,* 2001.

[11] C.G. Atkeson, J.G. Hale, F. Pollick, M. Riley, S. Kotosaka, S. Schaal, T. Shibata, G. Tevatia, A. Ude, S. Vijayakumar, and M. Kawato, "Using Humanoid Robots to Study Human Behavior," *IEEE Intelligent Systems,* vol. 15, no. 4, pp. 46-56, July/Aug. 2000.

[12] R.O. Ambrose, H. Aldridge, R.S. Askew, R. Burridge, W. Bluethman, M.A. Diftler, C. Lovchik, D. Magruder, and F. Rehnmark, "ROBONAUT: NASA's Space Humanoid," *IEEE Intelligent Systems,* vol. 15, no. 4, July/Aug. 2000.

[13] M.A. Diftler and R.O. Ambrose, "ROBONAUT, A Robotic Astronaut Assistant," *Proc. Int'l Symp. Artificial Intelligence, Robotics, and Automation in Space,* June 2001.

[14] W. Bluethmann, R. Ambrose, M. Diftler, S. Askew, E. Huber, M. Goza, F. Rehnmark, C. Lovchik, and D. Magruder, "Robonaut, a Robot Designed to Work with Humans in Space," *Autonomous Robots,* vol. 14, pp. 179-197, 2003.

[15] D.A. Winter, *Biomechanics and Motor Control of Human Movement,* second ed. New York: Wiley, 1990.

[16] M. Rosheim, *Robot Evolution: The Development of Anthrobotics.* New York: Wiley, 1994.

[17] V.M. Zatsiorsky, "Kinematics of Human Motion," *Human Kinetics,* Urbana, Ill., 1998.

[18] S. Tachi and T. Sakaki, "Impedance Controlled Master Slave Manipulation System Part I: Basic Concept and Application to the System with Time Delay," *J. Robotics Soc. Japan,* vol. 8, no. 3, pp. 241-252, 1990.

Riichiro Tadakuma received the BEng degree with First Class Honors in mechano-aerospace engineering from the Tokyo Institute of Technology in 2000 and the MEng degree in mechanical and aerospace engineering from the Tokyo Institute of Technology in 2002. He received the PhD degree in advanced interdisciplinary studies from the University of Tokyo in 2005. He is a research fellow of the University of Tokyo with a fellowship from the Japan Science and Technology Agency. He was a research fellow of the Japan Society for the Promotion of Science from 2003 to 2005. He was awarded the Hatakeyama Award from the Japanese Society of Mechanical Engineers (JSME) in 2000. His research interests includes robotics, telexistence, and virtual reality.

Yoshiaki Asahara received the BSci degree from the Department of Earth and Planetary Science at the University of Tokyo in 2002 and the MEng degrees in information physics and computing from the University of Tokyo in 2004. He has worked at Toyota Motor Corporation, Aichi, Japan, as an engineer.

Hiroyuki Kajimoto received the MS and PhD degrees in mathematical engineering and information physics from the University of Tokyo. He is a research associate in the Department of Information Physics and Computing at the University of Tokyo. His research interests include tactile displays, tactile sensors, and virtual reality.

Naoki Kawakami received the PhD degree in advanced interdisciplinary studies from the University of Tokyo. He is a lecturer in the Department of Information Physics and Computing at the University of Tokyo. His research interest is virtual reality.

Susumu Tachi received the PhD degree in mathematical engineering and information physics from the University of Tokyo. He is a professor in the Department of Information Physics and Computing at the University of Tokyo. He is a founding director of the Robotics Society of Japan (RSJ), a fellow of the Society of Instrument and Control Engineers (SICE), and is the founding president of the Virtual Reality Society of Japan (VRSJ). His research interests include virtual reality, telexistence, augmented reality, and robotics. He is a member of the IEEE.